Journal of Alloys and Compounds 507 (2010) 190–195

Contents lists available at ScienceDirect

Journal of Alloys and Compounds

journal homepage: www.elsevier.com/locate/jallcom

Temperature and voltage dependent current-transport mechanisms in GaAs/AlGaAs single-quantum-well lasers

H. Uslu[a,*], A. Bengi[a], S.Ş. Çetin[a], U. Aydemir[a], Ş. Altındal[a], S.T. Aghaliyeva[b], S. Özçelik[a]

[a] Physics Department, Faculty of Arts and Sciences, Gazi University, Ankara, Turkey
[b] National Academy of Science, Institute of Physics, Baku, Azerbaijan

ARTICLE INFO

Article history:
Received 20 April 2010
Received in revised form 17 July 2010
Accepted 21 July 2010
Available online 30 July 2010

Keywords:
QW lasers
I–V–T characteristics
Current-transport mechanism

ABSTRACT

The quantum-well (QW) lasers are the most important optoelectronic devices in many application fields and the current-transport mechanisms (CTMs) are strongly depend on temperature and voltage. Therefore, we have examined the samples in the temperature range of 80–360 K. The electrical parameters such as saturation current (I_o), zero-bias barrier height (Φ_{Bo}), ideality factor (n) and series resistance (R_s), were obtained from the forward bias *I–V* data. The n and Φ_{Bo} values change from 3.49 and 1.313 eV (at 80 K) to 1.73 and 0.492 eV (at 360 K), respectively. These values of n indicate that the thermionic field emission (TFE) mechanism is dominated the others, particularly at low temperature (80–170 K). High values of n were attributed to image force lowering of the barrier height, tunneling current at low temperature, generation-recombination current within the space charge region and the existence of interface states at metal/semiconductor interface. The Φ_{Bo} values do not have to be absolutely correct, especially when there are more CTMs present in a given temperature interval. Also, n and R_s were found to be extremely dependent on the contributions of particular CTMs to the total current; the ratio of which to the TE theory increases with the increasing temperature. The Φ_{Bo} and activation energy (E_a) values decrease with the linearly increasing temperature and voltage. In addition, double-logarithmic plots of the forward bias *I–V* characteristics have shown two distinct linear regions in the whole temperature range. SCLC mechanism may be dominated CTMs especially at high temperature regime namely regime II.

1. Introduction

Gallium arsenide (GaAs)-based structures are used as a basic component for high speed electronic, optoelectronic, low power devices and quantum-well (QW) detectors and lasers [1–5]. The GaAs well layers are doped with n-type dopant (Si) to provide electrons in the ground states of the wells. The QW formed by the conduction band discontinuity of AlGaAs and GaAs is in the scope of interest as it is deeper than the one formed by the valance band discontinuity; therefore it should be observed at higher temperature. The basic condition to detect this QW successfully is its location in the n-type part of the depletion layer of a reverse biased p–n junction or Schottky barrier on n-type semiconductor [6]. In electronic devices such as metal–semiconductor (MS) Schottky diodes, metal–insulator–semiconductor (MIS) structures, solar cells and p–n junctions, a number of current-transport mechanisms such as Thermionic Emission (TE), Thermionic Field Emission (TFE), Generation-Recombination (GR), minority carrier injection, multistep tunneling and leakage current, compete usually, one of them may dominate over the others in a certain temperature and voltage region. However, simultaneous contribution from two or more mechanisms could also be possible. In such devices the predominant CTMs depend on various parameters such as process of surface preparation, formation of barrier height (BH) at metal/semiconductor (M/S) interface, carrier concentration in semiconductor, density of surface states, sample temperature and applied bias voltage. Also, Schottky barrier height (SBH), n, native or deposited insulator layer at M/S interface and R_s are fundamental parameters of these devices and they strongly affect device performance [7–14]. Usually, the forward bias *I–V* characteristics are linear in the semi-logarithmic scale at intermediate bias voltage ($0.1\,V < V < 0.7\,V$) but deviate from linearity considerably especially due to the effect of R_s when applied voltage is sufficiently high [15].

There are many methods of determining the SBH based on *I–V*, *C–V* and photoelectric measurements in the literature [15–29]. Detailed knowledge of the current-transport process involved is essential in order to extract the barrier parameters, namely, BH, n and R_s. It is well known the analysis of the *I–V* characteristics of a device measured only at room temperature does not give a detailed information about the current-transport process and the nature of the barrier formed at the M/S interface. On the other hand, the forward bias *I–V* characteristics at wide temperature range allow us to

* Corresponding author. Tel.: +90 312 202 11 31; fax: +90 312 212 22 79.
E-mail address: h.uslu@gazi.edu.tr (H. Uslu).

0925-8388/$ – see front matter © 2010 Elsevier B.V. All rights reserved.
doi:10.1016/j.jallcom.2010.07.152

understand different aspects of CTMs. In addition, there are many methods of determining the R_s of devices [30–33] but the theoretical expression of R_s is still unclarified in the literature. In our calculations, we have applied the Ohm's Law ($R_i = \delta V_i/\delta I_i$).

In this study, the CTMs of GaAs/Al_xGa_{1-x}As SQW lasers have been investigated using forward and reverse bias *I–V* measurements methods in the temperature range of 80–360 K. The main aim of this study is to present some interesting electrical characteristics such as predominant CTMs, effect of the temperature and R_s. The analysis of the experimental data of our devices indicated that the CTM was controlled by TFE mechanism below 170 K and TE mechanism above 200 K.

2. Experimental details

The GaAs/Al_xGa_{1-x}As single-quantum-well (SQW) laser was grown on Zn doped p-type GaAs (1 0 0) substrate by solid source V80H molecular beam epitaxy (MBE) system. Prior to growth of the SQW laser structure, the substrate was cleaned conventionally using acetone, methanol and deionized water. After the cleaning step, the substrate were mounted on the molybdenum free substrate holder and loaded in the system using fast entry lock. The substrate was transferred to outgas stage and heated up to 400 °C for 2 h to ensure the removal of any residual organics. After the outgas process, the substrate was transferred to deposition chamber and mounted on the manipulator. Then, the substrate was heated up to 690 °C for the oxide desorption. After observing the fully oxide desorption, the substrate temperature was reduced to 660 °C. After reducing the substrate temperature, 0.5 μm Be doped ($p_{Be} = 1 \times 10^{18}$ cm^{-3}) p-type GaAs buffer layer was grown at a constant growth rate of 2.780 Å/s. The active layer was sandwiched between 1 μm Si doped ($n_{Si} = 5 \times 10^{17}$ cm^{-3}) n-type and Be doped ($p_{Be} = 1 \times 10^{18}$ cm^{-3}) p-type $Al_{0.6}Ga_{0.4}$As cladding layers and composed of 50 Å thickness single intrinsic i-GaAs quantum-well layer and 150 Å thickness Al_xGa_{1-x}As (x = 0.20–0.60) continuously graded-index separate-confinement-heterostructure (GRINSCH) barrier layers. Cladding, quantum-well and barrier layers were grown at a constant growth rate of 0.447 Å/s for AlAs and 0.670 Å/s for GaAs. Finally, 0.25 μm heavily Si doped ($n_{Si} = 1 \times 10^{18}$ cm^{-3}) n-type GaAs contact layer was then grown at 660 °C at a constant rate of 2.780 Å/s to complete the growth. Fig. 1(a) and (b) show the schematic conduction band diagram and the whole GaAs/Al_xGa_{1-x}As SQW laser structure of the processed device.

For the electrical characterization of the device, the top and bottom ohmic contacts were formed by deposition of metals using thermal evaporation system (Bestec, Germany) whose base pressure is 10^{-8} mbar. The evaporating system has four crucibles for metal sources. After the small pieces of Au, Ni metals and Au–Ge alloy were loaded in the different crucibles at the same time, the deposition chamber was pumped to reach the desired base pressure. To form the bottom contact, firstly, Au–Ge alloy with the thicknesses of 1000 Å was deposited at 400 °C substrate temperatures with a growth rate of 2.4 Å/s. Secondly, Au metals with the thicknesses of 600 Å were deposited on the Au–Ge contact with a growth rate of 2.2 Å/s. After the formation of bottom contact the 1 mm diameter dot shaped top contact with the thicknesses of 350/500/350/1750 Å were formed by deposition of Ni/Au–Ge/Ni/Au metals growth rates of 6.0/2.0/2.0/3.6 Å/s, respectively. After the top and bottom metallization processes the sample was annealed at 425 °C for 25 s in a nitrogen ambient atmosphere in order to form the ohmic contacts. Then, the silver paste was used to connect wires to the sample in order to prepare it for *I–V* measurements.

The *I–V* measurements were performed using Keithley 220 programmable constant current source and Keithley 614 electrometer. The *I–V* characteristics of these devices were measured in the temperature range of 80–360 K using a temperature controlled Janis vpf-475 cryostat, which enables us to make measurements in the temperature range of 77–450 K. The sample temperature was always monitored using a copper-constantan thermocouple close to the sample and measured with a dmm/scanner Keithley model 199 and a Lake Shore model 321 auto-tuning temperature controllers with sensitivity better than ±0.1 K.

3. Results and discussion

The method most frequently used in the practice pre-assumed pure TE (n = 1 and R_s = 0) over the barrier [15,16,34–37]:

$$I_{TE} = I_o \left[\exp\left(\frac{qV}{kT}\right) - 1\right] \tag{1a}$$

When the value of n is greater than unity and R_s of device sufficiently high, Eq. (1a) can be modified as:

$$I_{TE} = I_o \left[\exp\left(\frac{q(V - IR_s)}{nkT}\right)\right]\left\{1 - \exp\left[\frac{q(V - IR_s)}{kT}\right]\right\} \tag{1b}$$

Table 1
Temperature dependent values of various parameters determined from forward bias *I–V* characteristics of GaAs/Al_xGa_{1-x}As SQW laser.

Sıcaklık (K)	I_o (A)	n	Φ_{Bo} (eV)	R_s (at 4 V) (Ω)
80	2.33×10^{-21}	3.490	1.260	72.08
110	3.38×10^{-17}	2.625	1.114	70.48
140	6.08×10^{-15}	2.120	0.997	68.34
170	3.00×10^{-13}	1.879	0.909	66.19
200	7.33×10^{-11}	1.839	0.780	64.27
230	2.04×10^{-9}	1.811	0.704	62.43
260	3.23×10^{-8}	1.819	0.641	60.45
290	2.97×10^{-7}	1.804	0.590	58.12
320	1.52×10^{-6}	1.771	0.555	56.29
340	3.84×10^{-6}	1.740	0.535	55.32
360	8.61×10^{-6}	1.730	0.517	54.68

where I_o is the reverse-saturation current and described by

$$I_o = A^* A T^2 \exp(-q\Phi_{Bo}/kT) \tag{2a}$$

where the quantities A^*, A, Φ_{Bo} are the effective Richardson constant which is equal to 8.16 A/cm^2 K^2 for n-type GaAs, the area of diode, the zero-bias barrier height respectively. The value of I_o is obtained from the intercept of ln I vs V plot at zero bias (V = 0) for each temperature. Once I_o is determined Φ_{Bo} is obtained by rewriting Eq. (2a) as:

$$\Phi_{Bo} = \frac{kT}{q} \ln\left[\frac{AA^*T^2}{I_o}\right] \tag{2b}$$

In the practice, situation is different from the ideal case (pure TE and modified TE) especially at low temperatures and with high doped semiconductors. Then, the total current can be rewritten as [8]:

$$I = I_{TE}\left\{\exp\left(\frac{q(V - IR_s)}{kT}\right) - 1\right\} + I_{GR}\left\{\exp\left(\frac{q(V - IR_s)}{2kT}\right) - 1\right\} + I_{Tun}\left\{\exp\left(\frac{q(V - IR_s)}{E_o}\right) - 1\right\} + \frac{V - IR_s}{R_{sh}} \tag{3}$$

Choosing the proper saturation currents I_{TE}, I_{GR}, I_{Tun}, the tunneling parameter E_o and resistances R_s and R_{sh} allows us to fit the experimental forward bias *I–V* plots in a wide range of applied biases and at various temperature values. In general, at higher temperature the TE and the GR are dominant whereas the tunneling (TFE and FE) and leakage currents become more significant at lower temperatures and for higher doped materials [8,38].

Fig. 2 shows the semi-logarithmic forward and reverse bias *I–V* plots in the temperature range of 80–360 K. It shows a good rectification behavior especially at low temperatures. However, it can be seen that the current rises slowly with the applied reverse bias and does not show any effect of saturation. The lack of saturation for a sample under reverse bias can be commonly explained in terms of image force lowering of barrier height and the existence of a native or deposited interfacial layer between the metal and semiconductor [15,16].

The ideality factor n accounts for the departure of the current-transport mechanism from the ideal TE theory and obtained by rewriting Eq. (1b) as:

$$n = \frac{q}{kT}\left(\frac{dV}{d(\ln I)}\right) \tag{4}$$

The experimental values of I_o, n and Φ_{Bo} of the device are given in Table 1 for each temperature. As can be seen in Table 1, both the values of n and Φ_{Bo} depend strongly on temperature and they decrease with the increasing temperature. The experimental values of n and Φ_{Bo} for the device range from 3.49 and 1.313 eV (at 80 K) to 1.73 and 0.492 eV (at 360 K), respectively.

The high value of n was attributed to image force lowering of the barrier height [39], tunneling current at low temperature [7,40],

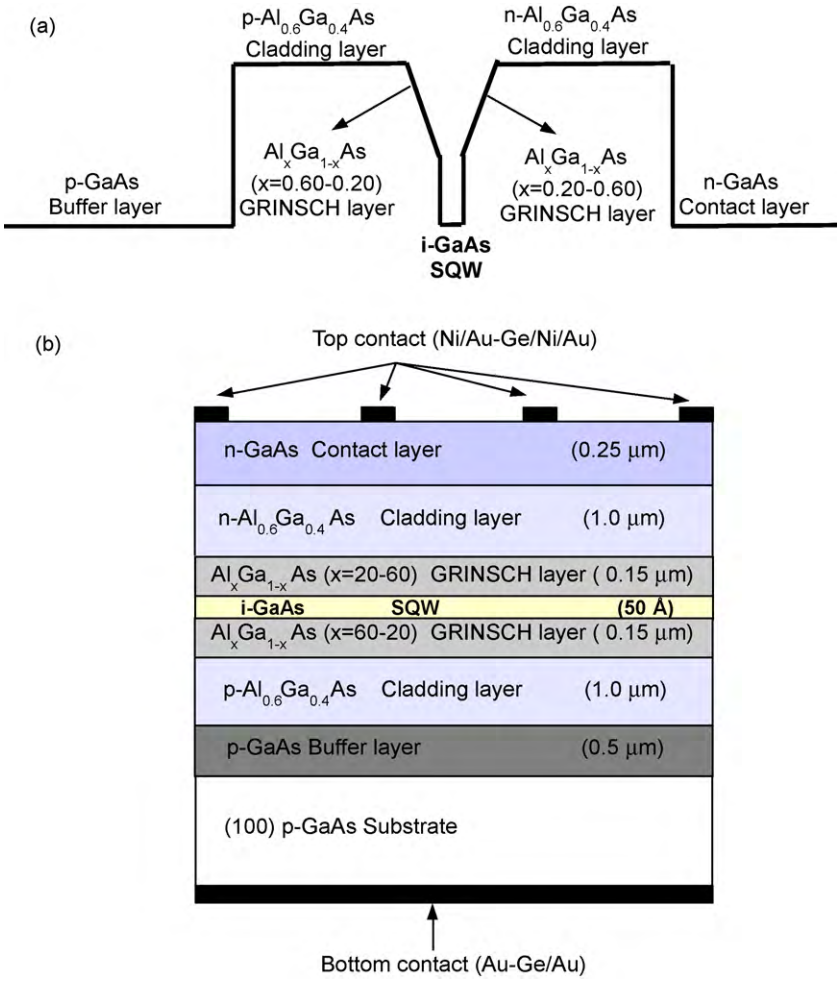

Fig. 1. (a) Schematic conduction band diagram for the GaAs/$Al_xGa_{1-x}As$ SQW laser structure. (b) Schematic diagram of the processed device.

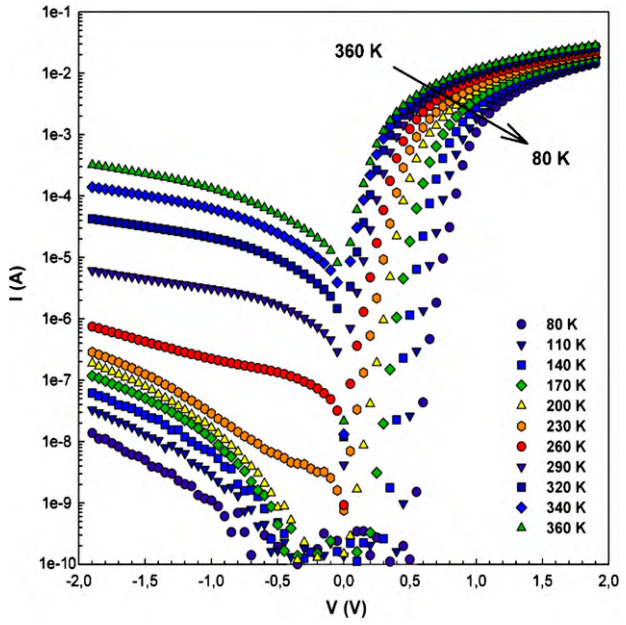

Fig. 2. The semi-logarithmic forward and reverse bias *I–V* characteristics of GaAs/$Al_xGa_{1-x}As$ SQW laser at various temperatures.

generation-recombination current within the space charge region [41] and the existence of interface states at metal/semiconductor interface [42,43].

The experimental n and Φ_{Bo} versus temperature plots are also given in Fig. 3(a) and (b), respectively. As shown in Fig. 3(b), the experimental data appear to fit, with two straight lines in different temperature regimes which are corresponds to low temperature region (between 80 and 170 K) and high temperature region (between 200 and 360 K), respectively. The value of Φ_{Bo} for two regimes decreases with the increasing temperature and can be described as

$$\Phi_{Bo}(T) = \Phi_{Bo}(T=0) - \alpha T \quad (5)$$

where Φ_{Bo} ($T=0$) is the barrier height extrapolated to zero temperature and α is the temperature coefficient of barrier height. In Fig. 3(b), the fitting of the Φ_{Bo} (T) yields Φ_{Bo} ($T=0$) = 1.07 eV and $\alpha = -16 \times 10^{-4}$ eV/K for low temperature region and Φ_{Bo} ($T=0$) = 1.55 eV and $\alpha = -39 \times 10^{-4}$ eV/K for high temperature region. This normal behavior can be attributed to the negative temperature coefficient (α) behavior of BH. The temperature dependence of BH can be explained as a result of Fermi level pinning mechanism that is governed either by metal induced band states [44] or by defect states at the interface [45]. There is a strong relation between the barrier height and the band gap ($\partial E_g/\partial T$) of the semiconductor. While the temperature increases, the band gap of semiconductor decreases, thus the barrier height decreases. The change in barrier height will be almost equal to the change

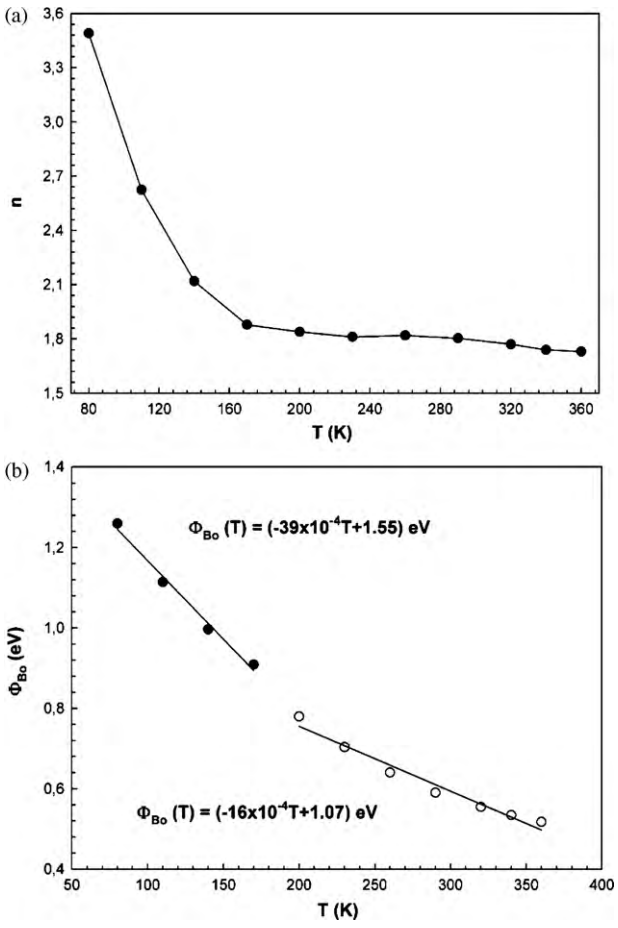

Fig. 3. Temperature dependent (a) n vs T. (b) Φ_{Bo} vs T of GaAs/Al_xGa_{1-x}As SQW laser.

in the band gap [11]. In addition, the decrease in BH with the increasing temperature is an evidence of the derivation from the pure Thermionic Emission (TE) to the Thermionic Field Emission (TFE) [46]. Here the negative temperature coefficient of the barrier height is found to be larger than that of the GaAs band gap of 5.405×10^{-4} eV/K in the temperature range of interest. Similar results have been reported in the literature [5,38,39].

Apart from discussing the main CTMs, the ideality factor is further analyzed by plotting nkT/q against kT/q in Fig. 4 which shows the experimental and theoretical results of this plot. As it can be

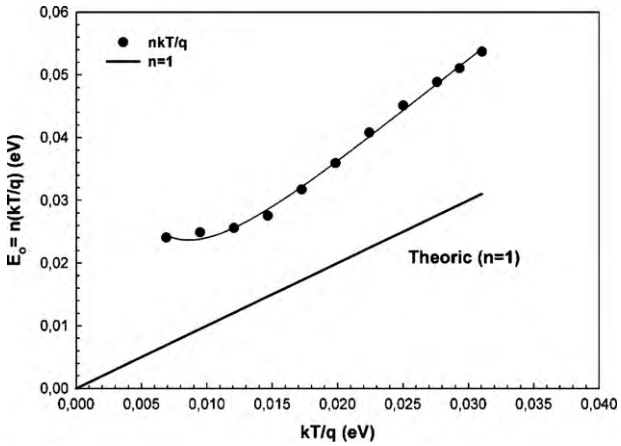

Fig. 4. Experimentally and theoretically found tunneling current parameter (E_o) vs kT/q for GaAs/Al_xGa_{1-x}As SQW laser.

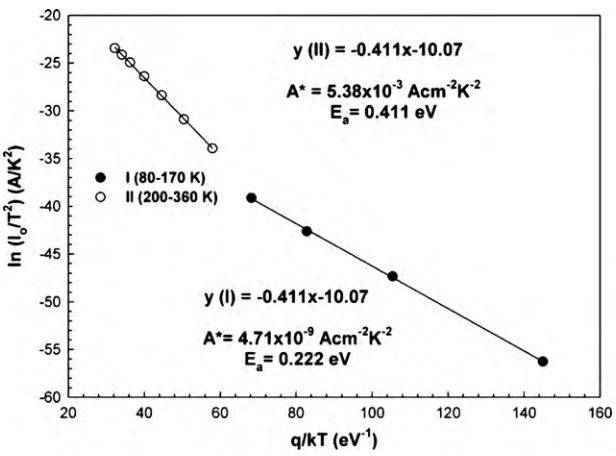

Fig. 5. Plot of $\ln(I_o/T^2)$ vs q/kT for GaAs/Al_xGa_{1-x}As SQW laser.

seen in Fig. 4 TFE is dominant mechanism in the temperature range of 80–170 K. The TFE requires a change in tunneling current parameter E_o with temperature according to relation [43,47]

$$E_o = nkT/q = E_{oo}\ \coth(qE_{oo}/kT) \tag{6}$$

with

$$E_{oo} = h/4\pi(N_D/m^*\varepsilon_s)^{1/2} \tag{7}$$

where $m^* = 0.067m_o$ is effective mass of electrons and $\varepsilon_s = 13.1\varepsilon_o$ the permittivity of GaAs and the other symbol are of usual meaning [3,15,16]. According to current-transport theory, TFE dominates only when $E_{oo} \cong kT/q$. n-GaAs with $\sim 6 \times 10^{22}$ m^{-3} doping concentration between 80 and 170 K (from C–V measurement) the value of E_{oo} was found as 4.8 meV and this calculated E_{oo} is close to the values of kT/q for the temperatures 80, 110, 140 and 170 K which correspond to 6.9, 9.49, 12.08 and 14.66 meV, respectively. But the values of E_{oo} for high temperatures are very less than the value of kT/q. In addition, the minority carrier is significant only for devices having very high saturation current with temperature independent ideality factor which has a value is very close to unity. The field emission (FE) theory is significant when nT is more or less constant in the temperature range, but in our sample the values of nT change with temperature. It is clear that for the CTMs in GaAs/Al_xGa_{1-x}As SQW laser, FE and minority carrier injection are ruled out. Therefore, we can say that the TFE transport mechanism is dominant at low temperatures while TE theory becomes dominant at high temperatures.

For the determination of the barrier height, one may also make use of the Richardson plot of the saturation current Eq. (2a) can be written as

$$\ln(I_o/T^2) = \ln(AA^*) - \left(\frac{q\Phi_{Bo}}{kT}\right) \tag{8}$$

The dependence of $\ln(I_o/T^2)$ vs q/kT is given in Fig. 5. As shown in Fig. 5, the $\ln(I_o/T^2)$ vs q/kT plot have two distinct linear regions with different slopes which correspond to low temperature region (between 80 and 170 K) and high temperature region (between 200 and 360 K), respectively. This implies that the BH is dependent on temperature, and two different CTMs may dominate in the whole temperature range. This plot yields a straight line with whose slope the $\Phi_{Bo}(=E_a)$ is determined and the intercept at the ordinate giving the Richardson constant itself for known A^* for two regimes. The experimental data appear to fit with two straight lines in different temperature regimes which correspond to low and high temperature regions, and the calculated activation energy values were found as 0.222 and 0.411 eV, respectively. Under forward bias and for $T > 200$ K, activation energy's having a value of

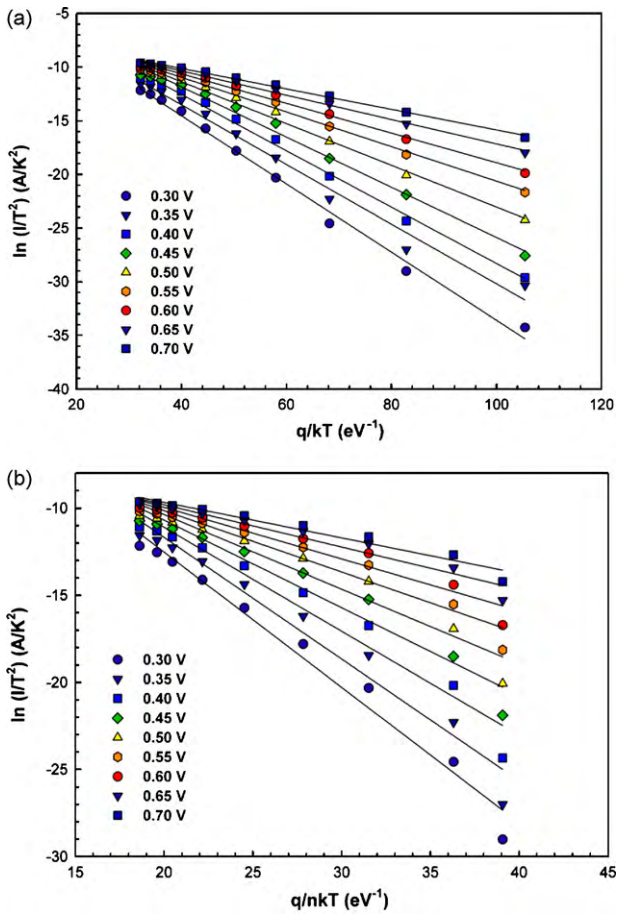

Fig. 6. Plot of (a) $\ln(I/T^2)$ vs q/kT. (b) $\ln(I/T^2)$ vs q/nkT for GaAs/Al_xGa_{1-x}As SQW laser.

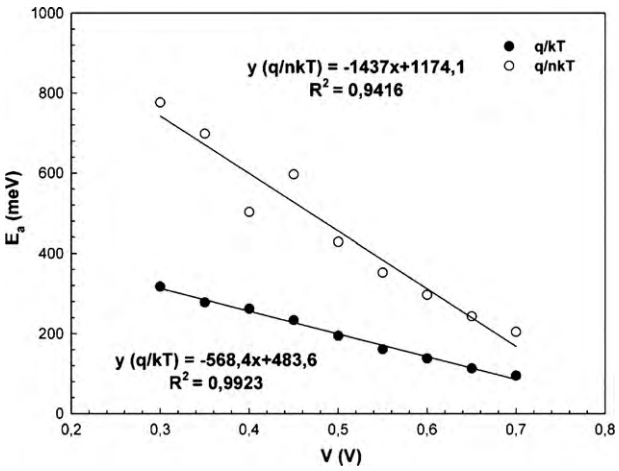

Fig. 7. Plot of activation energy vs applied bias voltage for GaAs/Al_xGa_{1-x}As SQW laser.

0.411 eV which is close to the half of the band gap in GaAs suggests that carrier TE (but $n > 1$) in the depletion layer plays a role above 200 K. However, at low temperatures ($T < 170$ K), the device shows a small activation energy (0.222 eV) when compared to usual value. The values of A^* obtained from the intercept of the straight portion for two regimes at the ordinate were found as 4.71×10^{-9} and 5.38×10^{-3} A cm^{-2} K^{-2}, which are much lower than the known value of 8.16 A cm^{-2} K^{-2} for n-GaAs. All these experimental results show that the predominant CTMs is not only the TE mechanism especially at low temperatures.

In order to interrupt the voltage dependent activation energy, we drew the activation energy plots ($\ln(I_o/T^2)$ vs q/kT and q/nkT) for GaAs/Al_xGa_{1-x}As SQW laser that is calculated from Eqs. (1a) and (4) and they are given in Fig. 6(a) and (b), respectively. As it can be seen activation energy plots are linear except for 80 K for various applied bias voltages (0.30–0.70 V). The experimental values of activation energy (E_a) obtained from Fig. 6(a) range from 0.318 eV (for 0.3 V) to 0.095 eV (for 0.7 V). On the other hand, these values of E_a obtained from Fig. 6(b) range from 0.777 eV (for 0.3 V) to 0.205 eV (for 0.7 V). These results show that the values of BH and E_a are strongly dependent on applied bias voltage especially at low temperatures. The obtained experimental values of E_a are given in Fig. 7 and they decrease with the increasing applied bias voltage. As shown in Fig. 7, the values of E_a are also lower than $E_g/2$ of GaAs at low bias voltages. These observations in E_a or Φ_{Bo} indicate that our results cannot be explained by the classical drift diffusion and by generation-recombination mechanisms. Similar results have been reported in the literature [48,49].

The forward bias $\ln(I)$ vs $\ln(V)$ plots at various temperatures are given in Fig. 8. As it can be seen from Fig. 8 $\ln(I)$ vs $\ln(V)$ plots can be characterized by two distinct linear regions, indicating different conduction mechanisms. At intermediate voltage region (I. regime) the values of slopes are strong function of temperature and they range from 26 (at 80 K) to 2.42 (at 360 K). At high voltage region (II. regime) the values of slopes are strong function of temperature and they range from 2.15 (at 80 K) to 1.40 (at 360 K). These results show that space charge-limited current (SCLC) mechanism is not the dominant mechanism especially in the low temperature regime (I. regime). However, SCLC mechanism may be dominated in the II. regime.

The series resistance (R_s) and shunt resistance (R_{sh}) are determined from the structure resistance (R_i) versus applied bias voltage (V_i) plot determined from the I–V characteristics by using Ohm's law ($R_i = dV_i/dI_i$) and they were given in Fig. 9. It was observed that at sufficiently high forward bias voltage the structure's resistance values approach to a constant value which corresponds to the series resistance (R_s) value for GaAs/Al_xGa_{1-x}As SQW lasers. Similarly, also at sufficiently high reverse bias voltage, the structure's resistance values reach to constant value, which is equal to structure's shunt resistance (R_{sh}). It is clear that the magnitude of the resistance values decreases with the increasing temperature according to literature [8,50–53]. It may be associated to the increase in the number of density of the free charge carriers, either by bond breaking or de-trapping mechanism [50].

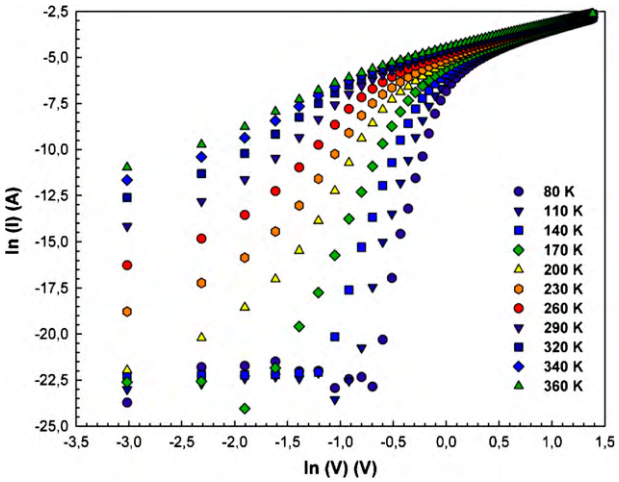

Fig. 8. Plot of $\ln(I)$ vs $\ln(V)$ for GaAs/Al_xGa_{1-x}As SQW laser.

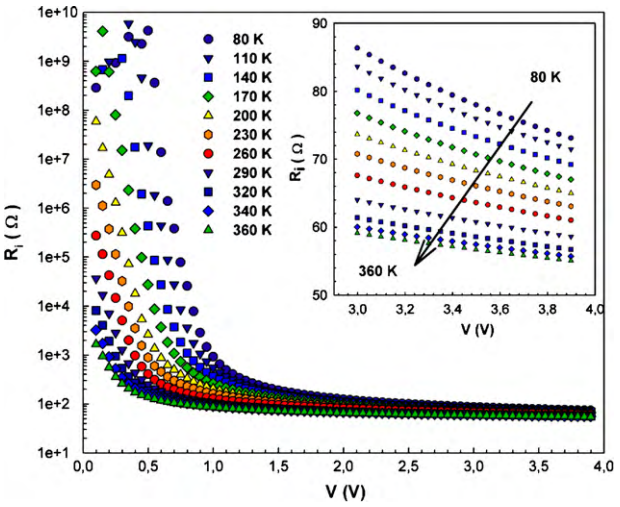

Fig. 9. The plot of the structure resistance vs applied bias voltage as a function of temperature for GaAs/$Al_xGa_{1-x}As$ SQW laser.

4. Conclusions

It is well known the quantum-well lasers are the most important optoelectronic devices in many application fields. Therefore, the forward and reverse bias *I–V* characteristics of GaAs/$Al_xGa_{1-x}As$ SQW lasers were measured in the temperature range of 80–360 K. The experimental semi-logarithmic *I–V* characteristics exhibit a linear behavior in the intermediate bias voltage region ($0.1 < V < 0.6$ V) and show a good rectifier behavior. The n, Φ_{Bo} and R_s obtained from forward bias *I–V* characteristics act as a function of temperature and applied bias voltage. The high values of n indicate that the sample obeys the thermionic field emission mechanism rather than the other transport mechanism particularly at low temperature (80–170 K). Also, such behavior of n can be attributed to image force lowering of the barrier height, tunneling current at low temperature, generation-recombination current within the space charge region and the existence of interface states at metal/semiconductor interface. Experimental results show that direct calculations of the Φ_{Bo} from experimental *I–V–T* characteristics do not have to be absolutely correct especially when there are more CTMs present in a given temperature interval. Also, the ideality factor and series resistance were shown to be extremely dependent on the contributions of particular CTMs to the total current; the ratio of which to the TE theory increases with the increasing temperature. It is observed that the values of Φ_{Bo} and E_a depend strongly on both temperature and applied forward bias voltage. The change in Φ_{Bo} and E_a decreases with linearly increasing temperature and applied bias voltage. In addition, double-logarithmic plots of the forward bias *I–V* characteristics of GaAs/$Al_xGa_{1-x}As$ SQW laser have shown two distinct linear regions/regimes at each temperature. At regime II, SCLC mechanism may be dominated current-transport mechanism especially in the high temperature regime.

Acknowledgements

This work is supported by TUBITAK under the 108T018 project number.

References

[1] C.C. Lee, W.V. Chen, J. Park, Microelectron. J. 37 (2006) 1335.
[2] C.H. Chen, S.M. Baier, D.K. Arch, M.S. Shur, IEEE Trans. Electron Devices 35 (1988) 570.
[3] M. Biber, Physica B 325 (2003) 138.
[4] C.S. Wu, C.P. Wen, R.N. Sato, M. Hu, C.W. Tu, J. Zhang, L.D. Flesner, L. Pham, P.S. Nayer, IEEE Trans. Electron Devices 39 (1992) 234.
[5] A. Bengi, Ş. Altındal, S. Özçelik, S.T. Agaliyeve, T.S. Mammadov, Vacuum 83 (2009) 276.
[6] K. Zdansky, V. Gorodynskyy, J. Kosikova, A. Rudra, E. Kapon, D. Fekete, Semicond. Sci. Technol. 19 (2004) 897.
[7] Ş. Altındal, İ. Dökme, M.M. Bülbül, N. Yalçın, T. Serin, Microelectron. Eng. 83 (2006) 499.
[8] D. Donoval, M. Barus, M. Zdimal, Solid State Electron. 34 (1991) 1365.
[9] S. Chand, J. Kumar, Semicond. Sci. Technol. 10 (1995) 1680.
[10] Ö. Vural, Y. Şafak, Ş. Altındal, A. Türüt, Curr. Appl. Phys. 10 (2010) 761.
[11] M.O. Aboelfotoh, Solid State Electron. 34 (1991) 51.
[12] A.K. Srivastava, B.M. Arora, S. Guha, Solid State Electron. 24 (1981) 185.
[13] A.F. Özdemir, A. Türüt, A. Kökçe, Semicond. Sci. Technol. 21 (2006) 298.
[14] M.D. Dio, A. Cola, M.G. Lupo, L. Vasanelli, Solid State Electron. 38 (1995) 1923.
[15] S.M. Sze, Physics of Semiconductor Devices, third ed., John Wiley&Sons, New York, 2007.
[16] E.H. Rhoderick, R.H. Williams, Metal–Semiconductor Contacts, 2nd ed., Clarendon Press, Oxford, 1988.
[17] R. Hackam, P. Harrop, IEEE Trans. Electron Devices 19 (1972) 1231.
[18] Ş. Aydoğan, K. Çınar, H. Asıl, C. Çoşkun, A. Türüt, J. Alloys Compd. 476 (2009) 913.
[19] K. Ejderha, N. Yıldırım, B. Abay, A. Turut, J. Alloys Compd. 484 (2009) 870.
[20] A. Tataroğlu, Ş. Altındal, J. Alloys Compd. 484 (2009) 405.
[21] A. Tataroğlu, Ş. Altındal, J. Alloys Compd. 479 (2009) 893.
[22] A. Sertap Kavasoglu, F. Yakuphanoglu, N. Kavasoglu, O. Pakma, O. Birgi, S. Oktik, J. Alloys Compd. 492 (2010) 421.
[23] A.A.M. Farag, A. Ashery, E.M.A. Ahmed, M.A. Salem, J. Alloys Compd. 495 (2010) 116.
[24] A.A.M. Farag, F.S. Terra, G.M. Mahmoud, A.M. Mansour, J. Alloys Compd. 481 (2009) 427.
[25] W.E. Mahmoud, A.A. Al-Ghamdi, E. El-Tantawy, S. Al-Heniti, J. Alloys Compd. 485 (2009) 59.
[26] V. Janardhanam, H.L. Lee, K.H. Shim, H.B. Hong, S.H. Lee, J. Alloys Compd. (2010), doi:10.1016/j.jallcom.2010.05.074.
[27] E. Bacaksiz, G. Çankaya, İ. Polat, S. Yılmaz, C. Duran, M. Altunbaş, J. Alloys Compd. 496 (2010) 560.
[28] V. Janardhanam, A.A. Kumar, V.R. Reddy, P.N. Reddy, J. Alloys Compd. 485 (2009) 467.
[29] İ.Y. Erdoğan, Ö. Güllü, J. Alloys Compd. 492 (2010) 378.
[30] H. Norde, J. Appl. Phys. 50 (1979) 5052.
[31] K. Sato, Y. Yasamura, J. Appl. Phys. 58 (1985) 3655.
[32] K. Cheung, N.W. Cheung, Appl. Phys. Lett. 49 (1986) 85.
[33] E.H. Nicollian, J.R. Brews, MOS Physics and Technology, New York, John Wiley & Sons, 1982.
[34] T.V. Blank, Y.A. Goldberg, Semiconductors 41 (2007) 1281.
[35] H. Bayhan, A.S. Kavasoglu, Solid State Electron. 49 (2005) 991.
[36] R.P. Raffaelle, H. Forsell, T. Potdevin, R. Friedfeld, J.G. Mantovani, S.G. Bailey, S.M. Hubbard, E.M. Gordon, A.F. Hepp, Sol. Energy Mater. Sol. Cells 57 (1999) 167.
[37] P. Kozodoy, J.P. Ibbetson, H. Marchand, P.T. Fini, S. Keller, J.S. Speck, S.P. DenBaars, U.K. Mishra, Appl. Phys. Lett. 73 (1998) 975.
[38] F.A. Padovani, R. Stratton, Solid State Electron. 9 (1966) 695.
[39] W.M.R. Divigalpitiya, Sol. Energy Mater. 4 (1989) 253.
[40] W.P. Kang, J.L. Davidson, Y. Gurbuz, D.V. Kerns, J. Appl. Phys. 78 (1995) 1101.
[41] P. Cova, A. Singh, Solid State Electron. 33 (1990) 11.
[42] H.C. Card, E.H. Rhoderick, J. Phys. D. Appl. Phys. 4 (1971) 1589.
[43] A. Singh, K.C. Reinhardt, W.A. Anderson, J. Appl. Phys. 68 (1990) 3475.
[44] J. Tersoff, Phys. Rev. Lett. 52 (1984) 465.
[45] J. Bardeen, Phys. Rev. B 71 (1947) 717.
[46] M. Soylu, B. Abay, Microelectron. Eng. 86 (2009) 88.
[47] S. Ashok, P.P. Sharma, S.J. Fonash, IEEE Trans. Electron Devices 27 (1980) 725.
[48] L. Hirsch, B. Barriere, J. Appl. Phys. 94 (2003) 5014.
[49] S. Mangal, P. Banerji, J. Appl. Phys. 105 (2009) 083709.
[50] K.S. Karimov, M.M. Ahmed, S.A. Moiz, M.I. Federov, Sol. Energy Mater. Sol. Cells 87 (2005) 61.
[51] Ş. Karataş, Ş. Altındal, A. Türüt, A. Özmen, Appl. Surf. Sci. 217 (2003) 250.
[52] S. Altındal, B. Sarı, H.I. Unal, N. Yavas, J. Appl. Polym. Sci. 113 (2009) 2955.
[53] F. Yakuphanoğlu, B.F. Şenkal, Synth. Met. 158 (2008) 821.